17th World Conference on Earthquake Engineering, 17WCEE
Sendai, Japan - September 13th to 18th 2020

EARTHQUAKE INTENSITY ESTIMATION BASED ON THE KRIGING METHOD CONSIDERING NEAR-FAULT FIELD EFFECTS

T. Koga[(1)], H. Wakamatsu[(2)], H. Sakai[(3)]

[(1)] *Hosei University, 2-33 Ichigayatamachi, Shinjuku, Tokyo 162-0843, Japan, tomoyuki.koga.9j@stu.hosei.ac.jp*
[(2)] *Keyence Corporation, 3-20-6 Myozincho, hachiozi-shi, Tokyo 192-0046, Japan, wakamatsu-h@sales.keyence.co.jp*
[(3)] *Hosei University, 2-33 Ichigayatamachi, Shinjuku, Tokyo 162-0843, Japan, hisakai@hosei.ac.jp*

Abstract

In Japan, severe earthquakes have triggered catastrophic damage to human beings and infrastructure. Therefore, infrastructure damage prediction is crucial and has been recently revised to more efficiently mitigate damages. Empirical damage predictions for roads, bridges, and underground buried pipelines typically use earthquake intensity measures, such as peak ground acceleration (PGA) and peak ground velocity (PGV). To improve existing empirical damage evaluation methods for infrastructure, measuring earthquake intensities with high accuracy at damaged structure sites is essential to relate structural damage with the earthquake intensity. However, earthquake values are usually not measured at damaged structure sites. Therefore, most earthquake intensity assessments are conducted based on the identified fault model using a three-dimensional ground structure based on the spline interpolation method and values at the observed sites along with some attenuation relationships. Today, the Kriging method is widely used to evaluate intensity distributions, but these measurements are not suitable for regions with sparse observation sites or those near the fault.

In the case of the 2016 Kumamoto earthquake, observation records were obtained near the fault, and the earthquake intensity distributions were measured through strong-motion evaluations based on the identified fault model.

In this study, we improve the Ordinary Kriging method by considering the characteristics near the fault region using the PGA distribution data from the 2016 Kumamoto earthquake. Assuming the random field was composed of a trend and random components, the negative effect of observational errors is reduced by interpolating only the random components based on the Kriging method. Specifically, we perform the following: 1) Calculation of every PGA on the engineering bedrock by dividing the PGA value with each site amplification factor. 2) Identification of the trend components of the random field by introducing the effects of asperity and directivity into the Ground motion prediction equation. 3) Interpolation of the PGA at the basement of each mesh point based on the Kriging method by calculating its difference with the trend component values as random components. 4) Calculation of the PGA distribution by adding the trend components to the random components and multiplying by each site amplification factor.

Our results confirm that the root mean squared error (RMSE) is acceptably small, and the estimation is performed with high accuracy. Furthermore, our results are comparable with those of a strong ground motion simulation as well as actual damage reports, thereby verifying their validity.

Keywords: Kriging method; earthquake intensity; asperity; directivity

1. Introduction

In recent years, frequent earthquakes, characterized by strong ground motions, have caused large scale damage to humans and infrastructure in Japan. Countermeasures against earthquakes are essential to reduce these damages. In order to estimate the damage to structures, detailed knowledge of the earthquake intensity is required. However, it is not possible to directly measure the earthquake intensity for all structures. Therefore, in order to estimate the earthquake intensity with high accuracy for each structure, it is necessary to extrapolate from the available seismograph results.

There are several methods of estimating earthquake intensity, including using ground motion simulations or a ground motion prediction equation. One method is to interpolate the earthquake intensity using the Kriging method, which is easier to handle than other methods because of its lower computational cost. This method is used by the Ministry of Land, Infrastructure, Transport, and Tourism in Japan to calculate the earthquake intensity distribution. However, the accuracy of the estimation deteriorates in areas where density of seismographs is insufficient or in areas near the fault affected by various factors such as asperity and the directivity effect.

The purpose of this study was to improve upon the existing method of estimating the earthquake intensity distribution, which uses the Kriging method, by considering the characteristics of ground motion near the fault. First, a program that considers the fault model and the ground parameters was created, and the earthquake intensity was estimated at an arbitrary point from the position data. Next, an earthquake intensity distribution map was created by repeating the estimation process for each 250 m mesh in the target area. Finally, the validity of the proposed method was examined by comparing the estimation results from this study with results from actual damage reports and ground motion simulations.

2. Kriging method

The Kriging method aims at predicting an unknown value at an arbitrary point from the distribution of the observed values, by minimizing the predicted error for that point. It is possible to predict the entire random field. Therefore, the Kriging method is utilized in various fields in science and engineering that require the quantitative evaluation of spatially correlated data.

This study examines the characteristics of ground motion near the fault, which cannot be considered, and assumes that the random field is eigen stationary. If the random field is eigen stationary, the variogram function can be expressed as

$$\gamma(h) = \sigma^2 \left\{ 1 - \exp\left(-\frac{h}{l} \right) \right\} \tag{1}$$

where, σ^2 is the variance of the data, h is the distance between any two points, and l is the autocorrelation distance. Assuming eigen stationarity, the proposed method uses the Ordinary Kriging method to make estimates. In the Ordinary Kriging method, the estimated value $Z(x_0)$ is interpolated by a linear combination of data $\sum w_i Z(x_i)$ $(i = 1 \sim n)$ using a variogram function. In this case, the weighting factor w_i is the solution to the following Ordinary Kriging equation, with a sum of 1.

$$Ax = y \tag{2}$$

$$A = \begin{bmatrix} 0 & \gamma(x_1 - x_2) & \cdots & \gamma(x_1 - x_n) & -1 \\ \gamma(x_2 - x_1) & 0 & \cdots & \gamma(x_2 - x_n) & -1 \\ \vdots & \vdots & \ddots & \vdots & \vdots \\ \gamma(x_n - x_1) & \gamma(x_n - x_2) & \cdots & 0 & -1 \\ -1 & -1 & -1 & -1 & 0 \end{bmatrix}$$

$$x = (\omega_1,\ \omega_2,\ \cdots,\ \omega_n,\ \lambda)^T$$
$$y = (\gamma(x_1 - x_0),\ \gamma(x_2 - x_0),\ \cdots,\ \gamma(x_n - x_0),\ -1)^T$$

where, λ represents Lagrange's undetermined multiplier. In the ordinary Kriging method, when the estimated position matches the sample position, the estimated value matches the sample data.

In this study, it was assumed that the random field is composed of a trend component and a random component, where the effect of the observation error is reduced by interpolating only the random component using the Kriging method. The random field is represented by the following equation:

$$Z(x) = \alpha Z(x) + \varepsilon(x) \tag{3}$$

where, $\alpha Z(x)$ is a trend component that is a definite value, and $\varepsilon(x)$ is a random component interpolated by the Kriging method.

3. Estimation method

3.1 Target area

In this study, we estimated the earthquake intensity distribution near the fault, using the main shock of the Kumamoto earthquake that occurred on April 25, 2016 at 1:25 am as the target earthquake. The estimated earthquake intensity was the peak ground acceleration (PGA) on the ground surface. The target area was a rectangular area of approximately 45 km by 65 km, excluding the sea area, within 32.6° to 33.0° N latitude and 130.5° to 131.2° E longitude, focusing on the area surrounding the Futagawa-Hinagu fault zone, which was the fault responsible for the Kumamoto earthquake.

We used the observation data from 77 sites in the strong motion observation network (KiK-net, K-net) of the National Research Institute for Earth Science and Disaster Resilience (NIED), the strong motion observation records of the Japan Meteorological Agency, and the seismographs of local governments within 32.5° to 33.1° N latitude and 130.4° to 131.3° E longitude.

3.2 Site amplification factors

In this study, the insufficient correlation distance density was improved upon by lowering the observation value obtained on the ground surface to the engineering bedrock by the site amplification factors. The site amplification factors were calculated using the estimation formula proposed by Yamaguchi and Midorikawa[1]. Yamaguchi and Midorikawa[1] extracted site amplification characteristics from a large number of records from a strong motion observation network, and formulated the change of their periodic characteristics using AVS30 as a parameter. The following equation represents the site amplification factors ARA_i.

$$ARA_i = 10^{\{g(x_s) - g(x_r)\}} \tag{4}$$
$$g(x) = \sum_{k=0}^{4} \frac{1}{k+1} a_k \cdot (\log x)^{k+1} \tag{5}$$

where, x_s is AVS30 (m/s), x_r is the S-wave velocity on the reference ground (m/s), and a_k is the regression coefficient as shown in Table 1. x_s uses the one published by J-SHIS of the NIED.

Table 1 - Regression coefficient a_k

k=0	-5.857×10^2
k=1	9.302×10^2
k=2	-5.490×10^2
k=3	1.428×10^2
k=4	-1.383×10

3.3 Ground motion prediction equation

In this study, we calculated the trend component of the PGA on the engineering bedrock using the ground motion prediction equation proposed by Tsukasa and Midorikawa[2].

$$\log A = b - \log X_{eq} - kX_{eq} \tag{6}$$

where, A is the PGA (Gal) , X_{eq} is the equivalent hypocenter distance (km) , and k is the coefficient representing the viscous damping, which was set to 0.003 by Tsukasa and Midorikawa[2]. b is expressed by the following equation.

$$b = aM_w + hP + \sum d_i s_i + e + \varepsilon \tag{7}$$

where, M_w is the moment magnitude, and P is the hypocenter depth, which, for the main shock of the Kumamoto earthquake were 7.0 and 12 km, respectively, according to the Japan Meteorological Agency. e is simply a constant term, with a value of 0.60. ε indicates the standard deviation, and 0.24 is used for points within 100 km from the hypocenter[2]. a, h, and d are regression coefficients, which have values of 0.5, 0.0036, and 0.00, respectively[2].

The equivalent hypocenter distance is defined as the distance from the point of a virtual hypocenter that emits energy equivalent to the energy received from the fault plane at any point, and is defined by the following equation[3].

$$X_{eq}{}^{-2} = \frac{\sum e_m X_m{}^{-2}}{\sum e_m} \tag{8}$$

where, X_m is the distance from the observation point to each small area m on the fault plane, and e_m is the relative emission of seismic energy from each small area m.

3.4 Directivity effect

The directivity effect is represented in the following formula of the directivity coefficient D, which refers to the method proposed by Oji et al[4].

$$D = \frac{1}{1 - (v/c) i_{rup} \cdot i_{ray}} \tag{9}$$

where, v is the rupture propagation velocity, c is the S-wave velocity of the earthquake basement, and $v/c = 0.72$[4]. i_{rup} and i_{ray} are the unit vectors in the direction of rupture and in the direction connecting the observation point to the hypocenter, respectively. Because the above equation is the inner product of these two vectors, the angle formed by each vector is converted to the following equation as θ.

$$D = \frac{1}{1 - (v/c)\cos\theta} \tag{10}$$

According to the research completed by Oji et al.[4], the directivity coefficient affects the equivalent hypocenter distance according to the following relation.

$$X_{eq}{}^{-2} = \frac{\sum e_m D_m X_m{}^{-2}}{\sum e_m} \tag{11}$$

Note that the directivity coefficient is 1 when there is no directivity effect.

3.5 Asperity

In this study, the fault model was set to reference the model used by Kubo et al.[5] for the source inversion analysis (Fig. 1). In addition, the fault plane was divided into 28 km in the strike direction and 12 small areas in the dip direction into a 2 km square area. Referring to the slip distribution map estimated by Kubo et al.[5] (Fig. 2), the position of the asperity was set in 37 small areas as shown in Fig. 3.

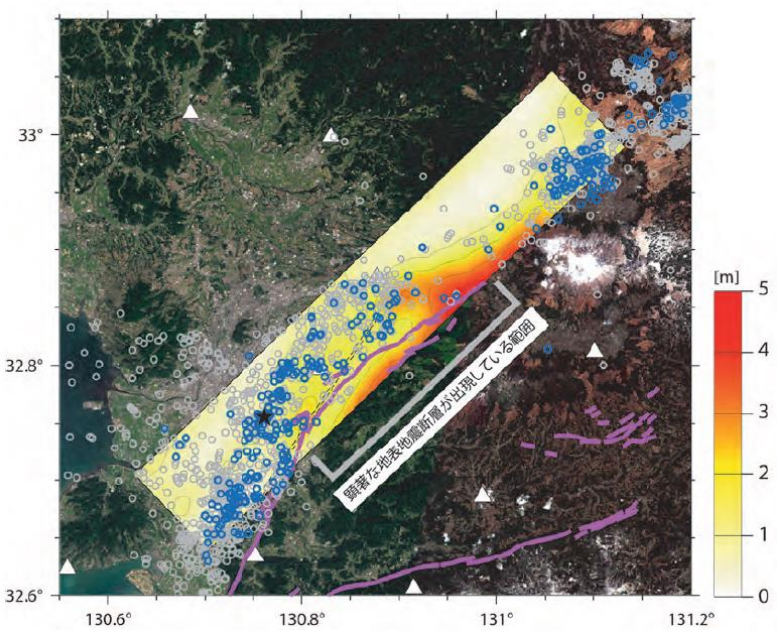

Fig. 1 - Fault model location[5]

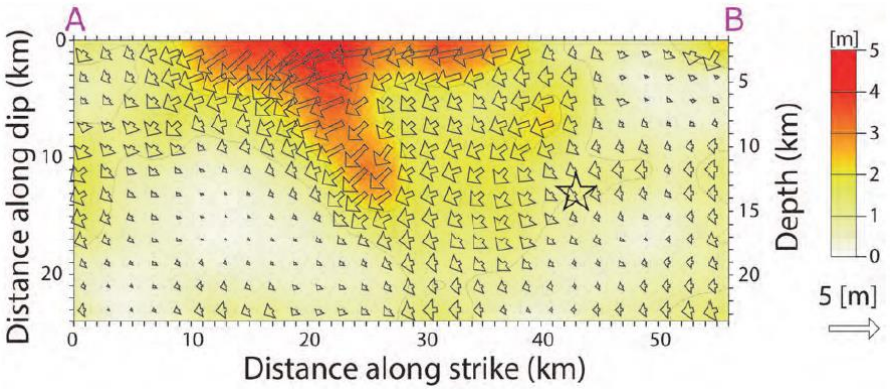

Fig. 2 - Fault plane slip distribution[5]

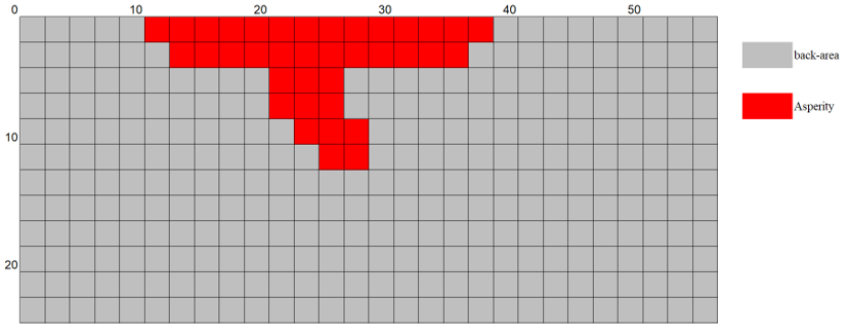

Fig. 3 - Small areas asperity

e_m from equation 7 is defined as the square of the slip level, according to Oji et al.[4] From "Recipe"[6], the average slip level of the entire asperity D_a (m) and the average slip level of the back-area D_b (m) are calculated as follows.

$$D_a = \xi \cdot D \tag{12}$$

$$D_b = M_{0b}/(\mu \cdot S_b) \tag{13}$$

where, D is the average slip level of the entire fault (m), M_{0b} is the earthquake moment in the back area (N・m), μ is the rigidity (N/m^2), and S_b is the area of the back-area (km^2). $\xi = 2$ from "Recipe"[6].

Using these indexes, the effect of the ground motion near the fault was incorporated into the equivalent hypocenter distance, and the trend component was calculated using the ground motion prediction equation. In order to calculate the distance in the program, the measurements of latitude and longitude were converted using 110.9463 km and 94.1978 km per degree, respectively.

4. Results of estimation

Table 2 shows the earthquake data used in the estimation. Based on the research by Tsukasa and Midorikawa[2], we made the assumption that $x_r = 600$ m/s, and estimated the mesh to be 250 m.

Table 2 - Earthquake data

Number of sample data	77
Fault rupture starting point latitude	32.7557
Fault rupture starting point longitude	130.7612
Depth to the Fault rupture starting point (km)	13.58
Fault dip (°)	65
Fault length (km)	56
Fault width (km)	24
Number of fault strike direction divisions	28
Number of fault dip direction divisions	12
Moment magnitude	7
Depth to the top of the fault rupture plane (km)	0.6
v/c	0.72
Fault strike (°)	226
Area of the asperity-area (km^2)	148
Area of the back-area (km^2)	1196
Earthquake moment (N・m)	5.3×10^{19}

Table 3 shows the estimation errors when the autocorrelation distance was set to 5 km, 10 km, 15 km, and 20 km.

Table 3 - Result of estimation

Autocorrelation distance	5km	10km	15km	20km
RMSE average	17.1 Gal	12.2 Gal	9.20 Gal	7.52 Gal
RMSE standard deviation	7.17 Gal	8.01 Gal	8.08 Gal	7.96 Gal

Table 3 shows that the accuracy showed the most improvement when the autocorrelation distance was set to 20 km. Fig. 4 and Fig. 5 show the estimated PGA distribution map and the root mean squared error (RMSE) distribution map when the autocorrelation distance was set to 20 km.

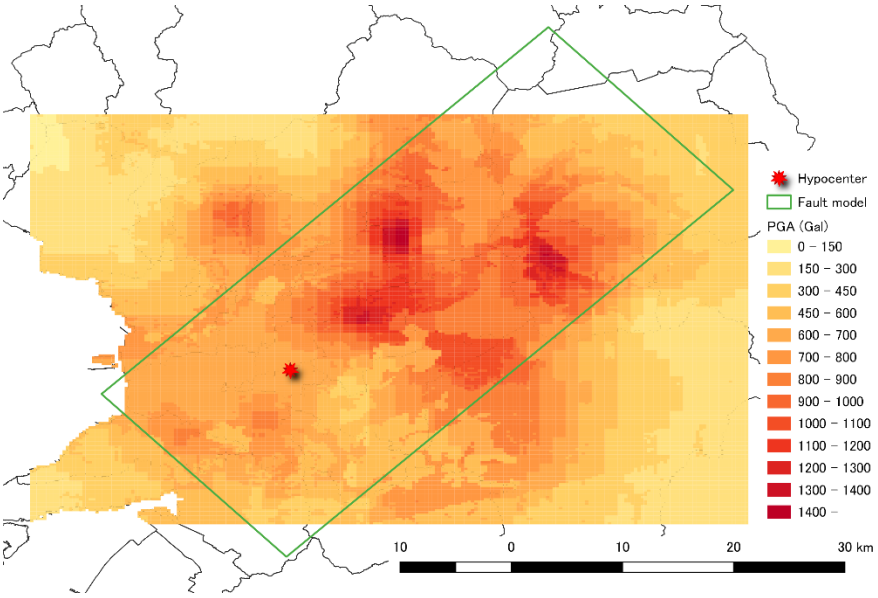

Fig. 4 - Estimated PGA distribution map (the autocorrelation distance 20km)

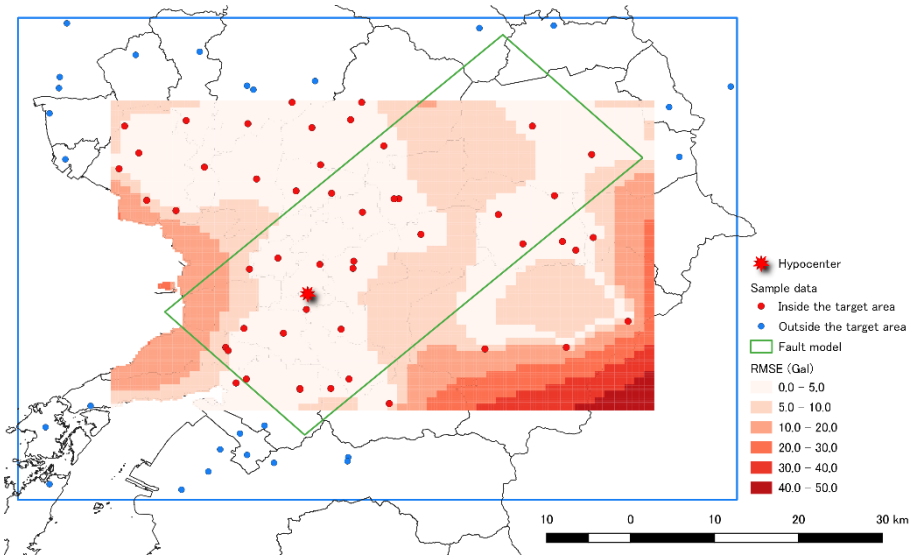

Fig. 5 - RMSE distribution map (the autocorrelation distance 20km)

From Fig. 4, it is clear that the PGA is larger at locations slightly further from the hypocenter, reflecting the effect of asperity. Additionally, the autocorrelation distance is an index that determines the range of influence of the observation point; there are instances where the sample data obtained is not sufficiently dense within the target area. Fig. 5 shows that the estimation error is small even in areas where the sample data was small when the autocorrelation distance was set to 20 km, therefore 20 km was utilized in the proposed method.

5. Examination of validity

5.1 Comparison with actual damage report

According to a study by Kagawa et al.[7], near the town of Mashiki, which was severely damaged, the Tabaru area, which is located nearby, was more severely damaged by the strong ground motion than the Kamizin and Shimozin areas near the surface earthquake fault. Fig. 6 shows an enlarged view of the estimated PGA

distribution map of the town of Mashiki. From this, it can be seen that a larger ground motion was predicted in the Tabaru area, as compared to the Kamizin and Shimozin areas.

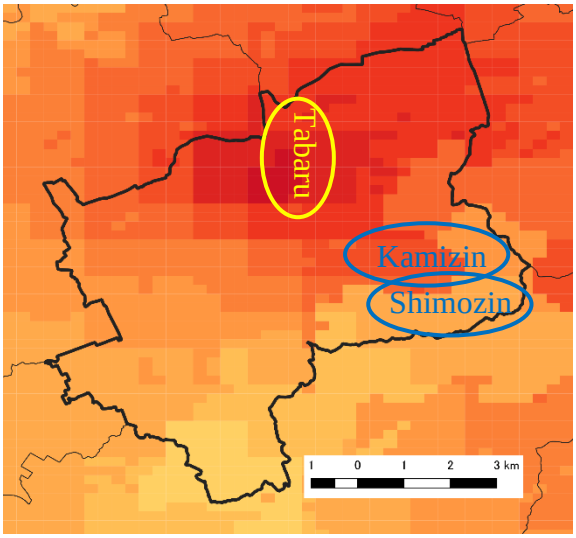

Fig. 6 - Enlarged map of estimated PGA distribution in Mashiki town

5.2 Comparison with ground motion simulation results

Fig. 7 shows the PGA distribution map obtained by Aoki[8] of the NIED using a ground motion simulation. This shows that the strong ground motion extends from the hypocenter in the east-west direction, particularly in the north-east direction, and a similar spread was confirmed by the estimation results.

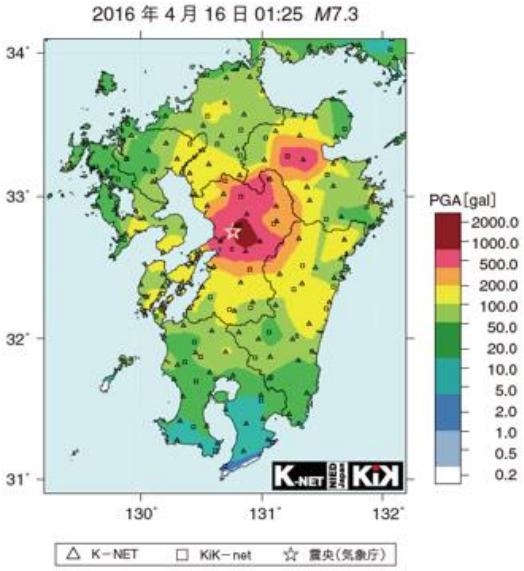

Fig. 7 - Aoki's PGA distribution map calculated by ground motion simulation[8]

6. Conclusions

In this study, we proposed a method of estimating the distribution of earthquake intensity utilizing the Kriging method and examined its validity. The estimation error was reduced by considering the asperity and directivity effects as characteristics of the ground motion near the fault, allowing for the accurate calculation of the PGA. The validity of this method was also confirmed by comparing actual damage reports and the results of strong ground motion simulations. However, there are additional features near the fault that may be significant, such as the hanging wall effect and the fling step. Therefore, it would be beneficial in the future to improve the accuracy of the ground motion prediction equation by including these factors.

Acknowledgments

In proceeding with this research, I referred to data published by the NIED, the Japan Meteorological Agency, Kumamoto Prefecture, Miyazaki Prefecture, Oita Prefecture, and Fukuoka Prefecture as sample data.

References

[1] M. YAMAGUCHI and S. MIDORIKAWA (2011) : Improvement of Method for Estimation of Site Amplification Factor Based on Average Shear-wave Velocity of Ground, Journal of Japan Association for Earthquake Engineering, Vol.11, No.3.

[2] H. SI and S. MIDORIKAWA (1999) : New attenuation relationships for peak ground acceleration and velocity considering effects of fault type and site condition, Journal of Architectural Institute of Japan, No.523, 63-70.

[3] A. MORIKAWA, K. KATO, T. IKEURA, M. TAKEMURA and A. OKAZAKI (2013) : Investigation of distance measuring indices to express hanging wall effect of peak ground accelerations in near source region of reverse fault – Applicability of equivalent fault distance and the shortest distance to fault plane - , Journal of Architectural Institute of Japan, Vol.78, No.694, 2073-2082.

[4] S. OJI, T. KANBARA, S. SAWADA and T. IWATA (2009) : Attenuation relationship by considered the effect of directivity based on equivalent hypocentral distance, Journal of Japan Society of Civil Engineers, A1, Vol.65, No.1, 104-110.

[5] H. KUBO, W. SUZUKI, S. AOI, H. SEKIGUCHI (2016) : Rupture process of the 2016 Kumamoto earthquake (Apr. 16, M 7.3) derived from near-source strong-motion records, National Research Institute for Earth Science and Disaster Resilience.

[6] The Headquarters for Earthquake Research Promotion (2017) : Strong ground motion prediction method for earthquakes with specified source faults (“Recipe”) .

[7] T. KAGAWA, S. YOSHIDA and H. UENO (2017) : Strong motion characteristics in the vicinity of surface fault rupture at suburbs of Mashiki town due to the 2016 Kumamoto earthquake, Journal of Japan Society of Civil Engineers, A1, Vol.73, No.4.

[8] S. AOI (2016) : Strong ground motion and hypocenter process of the 2016 Kumamoto earthquake, National Research Institute for Earth Science and Disaster Resilience.

